NLR surveillance of essential SEC-9 SNARE proteins induces programmed cell death upon allorecognition in filamentous fungi

Jens Heller[a,b], Corinne Clavé[c], Pierre Gladieux[d], Sven J. Saupe[c], and N. Louise Glass[a,b,1]

[a]The Plant and Microbial Biology Department, University of California, Berkeley, CA 94720-3102; [b]Environmental Genomics and Systems Biology Division, Lawrence Berkeley National Laboratory, Berkeley, CA 94720; [c]Institut de Biochimie et de Génétique Cellulaire, CNRS, Université de Bordeaux, 33077 Bordeaux, France; and [d]Biologie et Génétique des Interactions Plante-Parasite, University of Montpellier, Institut National de la Recherche Agronomique, Centre de Coopération Internationale en Recherche Agronomique pour le Dévelopement, Montpellier SupAgro, F-34398 Montpellier, France

Edited by John D. MacMicking, HHMI and Yale University School of Medicine, West Haven, CT, and accepted by Editorial Board Member Ruslan Medzhitov January 23, 2018 (received for review November 10, 2017)

In plants and metazoans, intracellular receptors that belong to the NOD-like receptor (NLR) family are major contributors to innate immunity. Filamentous fungal genomes contain large repertoires of genes encoding for proteins with similar architecture to plant and animal NLRs with mostly unknown function. Here, we identify and molecularly characterize patatin-like phospholipase-1 (PLP-1), an NLR-like protein containing an N-terminal patatin-like phospholipase domain, a nucleotide-binding domain (NBD), and a C-terminal tetratricopeptide repeat (TPR) domain. PLP-1 guards the essential SNARE protein SEC-9; genetic differences at *plp-1* and *sec-9* function to trigger allorecognition and cell death in two distantly related fungal species, *Neurospora crassa* and *Podospora anserina*. Analyses of *Neurospora* population samples revealed that *plp-1* and *sec-9* alleles are highly polymorphic, segregate into discrete haplotypes, and show transspecies polymorphism. Upon fusion between cells bearing incompatible *sec-9* and *plp-1* alleles, allorecognition and cell death are induced, which are dependent upon physical interaction between SEC-9 and PLP-1. The central NBD and patatin-like phospholipase activity of PLP-1 are essential for allorecognition and cell death, while the TPR domain and the polymorphic SNARE domain of SEC-9 function in conferring allelic specificity. Our data indicate that fungal NLR-like proteins function similar to NLR immune receptors in plants and animals, showing that NLRs are major contributors to innate immunity in plants and animals and for allorecognition in fungi.

allorecognition | NOD-like receptors | SEC-9 SNARE | *Neurospora* | *Podospora*

STAND-like NTPases are broadly distributed across all domains of life, potentially facilitated by horizontal gene transfer (1). In plants and metazoans, intracellular STAND-like NTPases of the nucleotide-binding domain (NBD), leucine-rich repeat (LRR) superfamily serve as sensors of pathogen-derived effector proteins (plants and metazoans) and pathogen-associated molecular patterns (metazoans), making them major constituents of innate immunity (2, 3). Upon pathogen recognition, these NOD-like receptors (NLRs) control programmed cell death (PCD) reactions in plants (hypersensitive response) and metazoans (apoptosis, pyroptosis, and necroptosis) to prevent the spread of the infection (3–5).

NLR proteins have a characteristic tripartite domain organization with a central NBD, an N-terminal downstream-acting domain, and C-terminal ligand-binding domains composed of superstructure-forming repeats (3). Despite similar modes of action of plant and metazoan NLRs and the involvement of related domains, phylogenetic analyses suggest that the typical domain architecture evolved de novo and independently (6). The genomes of filamentous fungi also encode genes with a core architecture similar to animal and plant NLRs. Some characterized fungal NLRs have been associated with a conspecific allorecognition process termed heterokaryon incompatibility (HI) (7, 8). During HI, heterokaryotic cells that are generated via cell fusion between genetically incompatible strains are rapidly compartmentalized and undergo PCD (7). HI has been shown to restrict mycovirus transfer between fungal colonies (9). Because an additional role for fungal NLR-like proteins during xenorecognition as part of a fungal innate immune system has been proposed (10, 11), an understanding of fungal NLR function could serve as a basis to study the general evolutionary origin of NLR-mediated pathogen defense and innate immunity.

Molecular models of NLR proteins are mostly based on studies in plants and metazoans. Intramolecular domain interactions are thought to keep NLRs in a suppressed state. Recognition of xenogeneous ligands [e.g., pathogen-associated molecular patterns, pathogen effectors (12)], as well as allogeneous ligands [e.g., during hybrid necrosis (13)], via C-terminal LRRs induces conformational changes that activate the NBD, thus initiating downstream reactions via functions of the N-terminal domains (14). Oligomerization can be part of the activation of animal NLRs (15). Several plant NLRs have also been hypothesized to form oligomers, although the function of the NBD for plant NLR oligomerization remains unresolved (16). The conserved domain architecture of NLRs across kingdoms suggests that similar modes of activation occur even if primary sequences and downstream functions can be diverse.

Significance

NOD-like receptors (NLRs) are fundamental components of plant and animal innate immune systems. Some fungal proteins with NLR-like architecture are involved in an allorecognition process that results in cell death, termed heterokaryon incompatibility. A role for fungal NLR-like proteins in pathogen defense has also been proposed. Here, we show that a fungal NLR-like protein, patatin-like phospholipase-1 (PLP-1), monitors the essential SNARE protein SEC-9 in two distantly related fungal species, *Neurospora crassa* and *Podospora anserina*. Both *plp-1* and *sec-9* are highly polymorphic in fungal populations and show evidence of balancing selection. This study provides biochemical evidence that fungal NLRs function similar to NLRs in plants and animals, indicating that these fundamental players of innate immunity evolved independently in all three kingdoms.

Author contributions: J.H., C.C., and N.L.G. designed research; J.H. and C.C. performed research; J.H., C.C., P.G., and S.J.S. analyzed data; and J.H., P.G., S.J.S., and N.L.G. wrote the paper.

The authors declare no conflict of interest.

This article is a PNAS Direct Submission. J.D.M. is a guest editor invited by the Editorial Board.

Data deposition: The sequence reported in this paper has been deposited in the GenBank database (accession no. SRP121656).

[1]To whom correspondence should be addressed. Email: lglass@berkeley.edu.

This article contains supporting information online at www.pnas.org/lookup/suppl/doi:10.1073/pnas.1719705115/-/DCSupplemental.

Published online February 20, 2018.

Here, we molecularly characterize a filamentous fungal NLR controlling an allorecognition and PCD process that acts at the germling stage (i.e., in germinated asexual spores), a process termed germling-regulated death (GRD). In a *Neurospora crassa* population, the GRD phenotype was associated with polymorphisms at the *sec-9* and *plp-1* loci. Cells from different GRD haplotypes (GRDHs) (and thus with alternative alleles at *sec-9* and *plp-1*) underwent rapid cell death following germling fusion. The *sec-9* locus encodes an essential SNARE protein, while *plp-1* encodes a fungal NLR. Coimmunoprecipitation (co-IP) experiments showed that interactions of incompatible SEC-9 and PLP-1 encoded by different haplogroups induce PLP-1 oligomerization associated with PCD. Additionally, we show that orthologs of *sec-9* and *plp*-1 in *Podospora anserina*, which diverged from *N. crassa* ∼75 Mya, also mediate allorecognition and PCD. These data indicate the importance of this NLR-based surveillance system of the SEC-9 SNARE in filamentous fungi and show that a common molecular mechanism underlies NLR function in animals, plants and fungi.

Results

GRD Haplotypes in an *N. crassa* Population Are Associated with Genomic Rearrangements and with Loci That Encode Highly Divergent Alleles. Analysis of germling communication phenotypes between wild isolates of an *N. crassa* population (17) revealed that some fused germling pairs between genetically different wild isolates die ∼20 min postfusion, as indicated by strong vacuolization, cessation of cytoplasmic flow, and uptake of the vital dye SYTOX Blue (Movies S1 and S2). We refer to this rapid cell death phenotype following fusion as GRD (Fig. 1).

Death rates of fused germlings were quantified using vital dyes and flow cytometry (*Materials and Methods* and Fig. S1 *A* and *B*). Germlings from single strains (self-fusion) showed death frequencies of ∼5%. When germlings of different GRD background were paired, death frequencies significantly increased (∼50%) (when mixed at a 1:1 ratio, an ∼50% germling death rate corresponds to the maximal death rate to be expected if all fused germlings of different GRD background die). Importantly, GRD was not germling-specific, but also occurred after fusion of mature hypha of a different GRD background. Analyses of the segregation of the GRD phenotype in F1 progeny from a cross between a GRD1 strain [Fungal Genetics Stock Center (FGSC) 2489] and a GRD3 strain (JW258) showed that the GRD phenotype segregated as a Mendelian trait.

To identify the GRD locus, we performed a bulk segregant analysis and whole-genome resequencing of progeny pools with an identical GRD phenotype from a backcross of F1 progeny with a GRD1 strain (FGSC 2489). Bulked segregant analysis revealed an ∼180-kbp region on the right arm of linkage group I (LGI) that showed segregation of SNPs between the different GRD phenotype pools at ∼100% frequency (Fig. S2*A*). A random SNP distribution was observed for the rest of LGI and for the remaining six LGs of *N. crassa*.

To further refine the GRD locus within the ∼180-kbp region, resequencing data from 23 wild isolates from this same *N. crassa* population were analyzed (18), revealing a 55-kbp region that showed four different genomic rearrangements spanning 21 loci [NCU09237 to NCU09253; gene nomenclature is based on the reference genome FGSC 2489 (19)]. We refer to these genomic rearrangements as GRD haplotypes 1 through 4 (GRDH1–4) (Fig. 2*A*). To determine whether structural differences between GRDHs were associated with nucleotide differences in particular genes, we used sequence alignments to characterize the nature and level of variability of genes within and between the haplogroups. Among the loci in the genetic interval associated with GRDHs, only NCU09243 and NCU09244 displayed high levels of allelic variability in the genomes of the 23 isolates (Fig. S2*B* and Table S1). Both genes were among the most polymorphic genes of the *N. crassa* population, in the top 0.1% for the number of polymorphic sites and nucleotide diversity (π; comparison with a set of 8,621 reference genes from ref. 18). High positive Tajima's D values indicated the presence of NCU09243 and NCU09244 alleles at an intermediate frequency

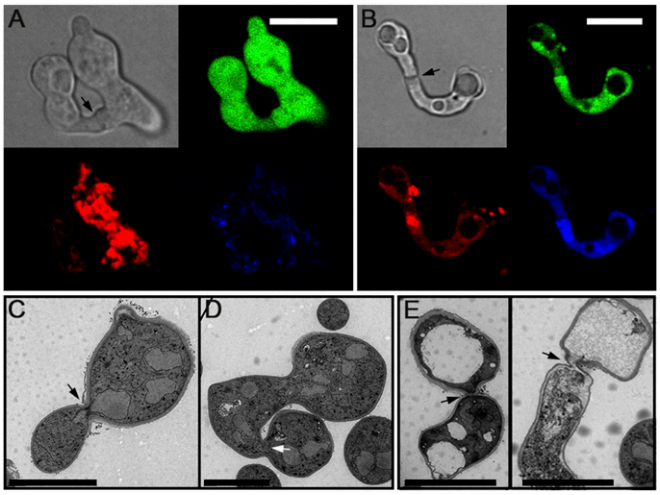

Fig. 1. GRD is induced if genetically incompatible germlings undergo cell fusion. (*A*) (*Top Left*) Brightfield image of a fused germling pair. When GRD1 germlings (FGSC 2489), marked with cytoplasmic GFP (green, *Top Right*), undergo cell fusion with FM4-64–stained GRD1 germlings of segregant 18 (red, *Bottom Left*), no death occurred, as indicated by the absence of SYTOX Blue fluorescence (*Bottom Right*). Note that fusion has occurred because GFP has entered segregant 18 (*Top Right*). (*B*) (*Top Left*) Brightfield image of a fused germling pair. When GRD1 germlings (FGSC 2489), marked with cytoplasmic GFP (green, *Top Right*), fused with FM4-64–stained GRD3 germlings of segregant 2 (red, *Bottom Left*), vacuolization and death occurred, as indicated by strong SYTOX Blue fluorescence (*Bottom Right*). Note that fusion has occurred because GFP has entered segregant 2 (*Top Right*). Transmission electron micrograph of GRD1 germlings (FGSC 2489) undergoing self-fusion (*C*) or segregant 2 germlings undergoing self-fusion (*D*) showed healthy cells with no signs of death. (*E*) In a mixture of GRD1 germlings (FGSC 2489) and GRD3 germlings (segregant 2), fused cells showed vacuolization, plasma membrane detachment from the cell wall, and organelle degradation. Arrows indicate fusion points. (Scale bars: 10 μm.)

in the population, and gene genealogies revealed four long-diverged haplogroups (Fig. 2 *A* and *B*, Fig. S2 *C* and *E*, and Table S2) that correlated with the genomic rearrangements of the four GRDHs. Alleles at NCU09243 and NCU09244 between members of different GRDHs were highly divergent, with nucleotide divergence per site ranging from 25 to 49%. In contrast, nucleotide diversity of NCU09243 and NCU09244 alleles within a single GRDH was two orders of magnitude lower than divergence between GRDHs (π ranging from 0 to 0.01105 per base pair), comparable with the rest of the genome (average π = 0.007416 per base pair, SD = 0.008449). All other genes in the 55-kbp region were significantly less polymorphic than NCU09243 and NCU09244 (Fig. S2 *B* and *C*), and gene genealogies did not show long-diverged haplotypes (Fig. 2 *A* and *B* and Fig. S2*D*). Exceptions were NCU09247 and NCU16494, which showed high Tajima's D values (D = 1.40 and D = 1.42, respectively), but haplotype groups in these genes did not track with GRDHs (Fig. S2 *C* and *D*). The GRDH2, GRDH3, and GRDH4 strains also contain a duplication of NCU09244, but are missing NCU09245, which is only present in GRDH1 strains (Fig. 2*A*). Both NCU09244 and NCU09245 encode proteins with predicted patatin-like phospholipase domains, suggesting they are paralogs, despite low total amino acid sequence identity (∼18%) (Table S1). In addition to the N-terminal patatin-like phospholipase domain, NCU09244 has an NBD [nucleotide-binding adaptor shared by Apaf-1, resistance proteins, and CED-4 (NB-ARC) type] and C-terminal tetratricopeptide repeats (TPRs), a domain structure described for NLRs (3, 10). We called this gene *plp-1*. NCU09245 has a similar structure to PLP-1 but is missing the NBD domain. NCU09245 was named *plp-2*.

NCU09243 has homology to the t-SNARE protein Sec9 of *Saccharomyces cerevisiae*, which is required for secretory vesicle/plasma

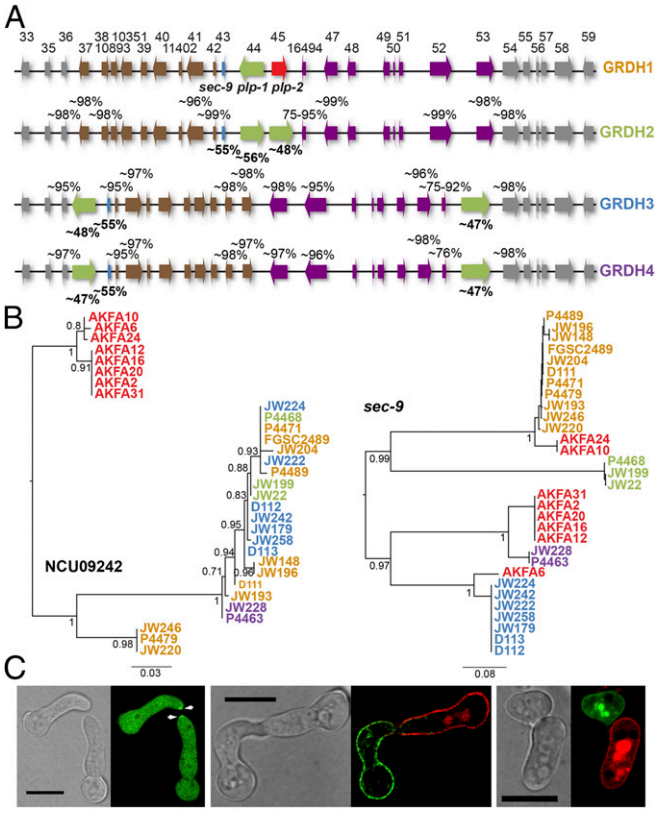

Fig. 2. *sec-9*, *plp-1*, and *plp-2* within the GRDH region show TSP. (*A*) Genomic organization of GRDH regions in *N. crassa* wild isolates. Genomic rearrangements within the GRDHs spanned the genetic interval between NCU09237 and NCU09253 (shown are the last two digits of NCU numbers) and included duplications of NCU09244, a deletion of NCU09245, and inversions. Alleles at NCU09243 (*sec-9*) and NCU09244 (*plp-1*) within a GRDH show high DNA sequence identity, but are diverse between GRDHs. The percentages of DNA identity between alleles in members of the different GRDH groups of selected genes across the genetic interval in comparison to FGSC 2489 (a member of GRDH1) are shown. (*B*) Coding sequences from 23 *N. crassa* wild Louisiana isolates and eight *N. discreta* wild isolates were used to build maximum likelihood phylogenetic trees for NCU09242 and NCU09243 (*sec-9*) using the default pipeline from Phylogeny.fr (63). Bootstrap values are given for each node. Black bars indicate substitution rates. GRDH1 isolates are shown in yellow, GRDH2 isolates are shown in green, GRDH3 isolates are shown in blue, and GRDH4 isolates are shown in purple. *N. discreta* isolates are shown in red. Note nesting of *N. discreta* isolates within *N. crassa* lineages for NCU09243 (*sec-9*), but not for NCU09242. Phylogenetic trees of NCU09244/NCU09245, NCU16494, and NCU09247 are shown in Fig. S2 *D* and *E*. (*C*, *Left*) SEC-9–GFP localizes to the cytoplasm and concentrates at a crescent at the tips of germ tubes (arrowheads). Cytosolic localization might reflect cleaved GFP as apparent from Western blot analyses (Fig. 6). (*C*, *Center*) PLP-1–GFP and PLP-1–mCherry predominantly localize to the periphery of the cell. (*C*, *Right*) PLP-2–GFP and PLP-2–mCherry also predominantly localize to the periphery of the cell. Localization to the vacuoles is common in mCherry-tagged proteins in *N. crassa*. (Scale bars: 10 μm.)

membrane fusion (20). We therefore named NCU09243 *sec-9*. The *plp-1* and *sec-9* genes of *N. crassa* are orthologs of *vic-2* and *vic-2a*, respectively, which confer *vic-2* vegetative incompatibility in the chestnut blight fungus *Cryphonectria parasitica* (21).

Alleles at *sec-9* and *plp-1/plp-2* Show Signatures of Balancing Selection. The finding of four highly divergent GRDHs suggested a relatively ancient origin of the GRD locus. To test this hypothesis, we performed phylogenetic analyses of alleles at NCU09242 through NCU09247 from the 23 wild *N. crassa* isolates, as well as alleles at these same loci from a population sample from the distantly related species *Neurospora discreta*. For NCU09242, NCU16494, and NCU09247, allelic lines from within species were reciprocally monophyletic (Fig. 2*B* and Fig. S2*D*), as predicted by theory (22), given the estimated divergence time between *N. crassa* and *N. discreta* [7–10 Mya (23)] and their effective population size [circa 10^6 and 10^4 individuals, respectively (24, 25)]. However, for *sec-9* and *plp-1*, no reciprocal monophyly was observed, indicating that the age of allelic lines exceeds the age of speciation events (Fig. 2*B* and Fig. S2*E*). This phenomenon is referred to as transspecies polymorphism (TSP) and has been observed in *N. crassa* for other loci involved in non–self-recognition (17, 18, 26). The observed pattern of TSP is consistent with balancing selection and limited recombination among alleles causing the evolution of highly divergent haplogroups. Inferred genealogical histories of *sec-9*, *plp-1*, and *plp-2* were, in fact, concordant with differences in patterns of genomic arrangements among GRDHs, suggesting limited recombination across the whole region: Alleles from GRDH1 to GRDH4 were in distinct clades for *sec-9* and *plp-1*/*plp-2* (*plp-2* was in a separate clade because it is only present in GRDH1 strains, while *plp-1.2* of GRDH3 and GRDH4 sequences clustered together) (Fig. 2*B* and Fig. S2*E*).

Nonallelic Genetic Interactions Between *plp-1* and *sec-9* Mediate GRD. Based on the evolutionary analyses of genes within the GRDHs, we hypothesized that genetic interactions between *sec-9* and/or *plp-1*/*plp-2* confer GRD. To test this hypothesis, we first examined strains carrying single deletions of *plp-1* or *plp-2* and strains bearing deletions of both *plp-1* and *plp-2* in a GRD1 background. The *Δplp-1*, *Δplp-2*, and *Δplp-1 Δplp-2* strains were macroscopically indistinguishable from their parental strains and displayed similar death frequencies in self-pairings (Fig. S1*C*). In allogenic (non-self) pairings, all three mutants (*Δplp-1*, *Δplp-2*, and *Δplp-1 Δplp-2*) displayed the GRD specificity of their isogenic GRD1 parent (i.e., ~50% germling death frequency when paired with a GRD3 strain) (Fig. 3*A*). These data indicated that GRD is not mediated by allelic interactions between *plp-1* or *plp-2* alleles, or by nonallelic *plp-1*/*plp-2* interactions.

Attempts to construct a *sec-9* deletion strain were unsuccessful, indicating *sec-9* is an essential gene in *N. crassa*, similar to *S. cerevisiae SEC9* (27). Therefore, we created swap strains where the *sec-9*^{GRD1} allele in a *Δplp-1 Δplp-2* strain (GRD1 background) was replaced with *sec-9* alleles from other haplogroups (GRDH2, GRDH3, or GRDH4) (Fig. 3*B*). All of these *sec-9* swap strains showed increased germling death frequencies when paired with the parental GRD1 strain (20–40%) (Fig. 3*C*). These data indicated that either allelic interactions between *sec-9* genes or nonallelic interactions between *sec-9* and *plp-1* and/or *plp-2* were required to induce GRD. To distinguish between these possibilities, we paired germlings containing alternate *sec-9* alleles, but which lacked both *plp-1* and *plp-2*; death frequencies in these pairings were similar to self-death frequencies (Fig. 3*C* and Fig. S1*C*), indicating that allelic differences at *sec-9* were not sufficient to induce allorecognition and germling death. To test if nonallelic interactions between *sec-9* and *plp-1* and/or *plp-2* are important for GRD, germling death frequencies were assessed when *sec-9* swap strains (*sec-9*^{GRD2}, *sec-9*^{GRD3}, or *sec-9*^{GRD4}, all in a *Δplp-1 Δplp-2* background) were paired with *sec-9*^{GRD1} strains bearing either a *Δplp-1* or *Δplp-2* deletion. Significantly, cell death rates were reduced in pairings with the *sec-9*^{GRD1} *Δplp-1* strain, but not in pairings with the *sec-9*^{GRD1} *Δplp-2* strain (Fig. 3*C*). These data indicated that nonallelic interactions between *sec-9* and *plp-1* mediate allorecognition and GRD.

The *sec-9*/*plp-1* nonallelic interactions among the different haplogroups were confirmed to be essential for GRD by analyzing cell death in pairings of a GRD3 strain with all *sec-9* swap strains. As expected, pairings between the GRD3 and *sec-9*^{GRD3} *Δplp-1 Δplp-2* germlings showed low death frequencies (~5%). In contrast, pairings between the GRD3 strain and the *sec-9*^{GRD1} *Δplp-1 Δplp-2* strain showed high death frequencies (~50%), as did pairings between the GRD3 strain and the *sec-9*^{GRD2} *Δplp-1 Δplp-2* strain. However, pairings between the GRD3 strain and the *sec-9*^{GRD4} *Δplp-1 Δplp-2* strain showed intermediate death frequencies

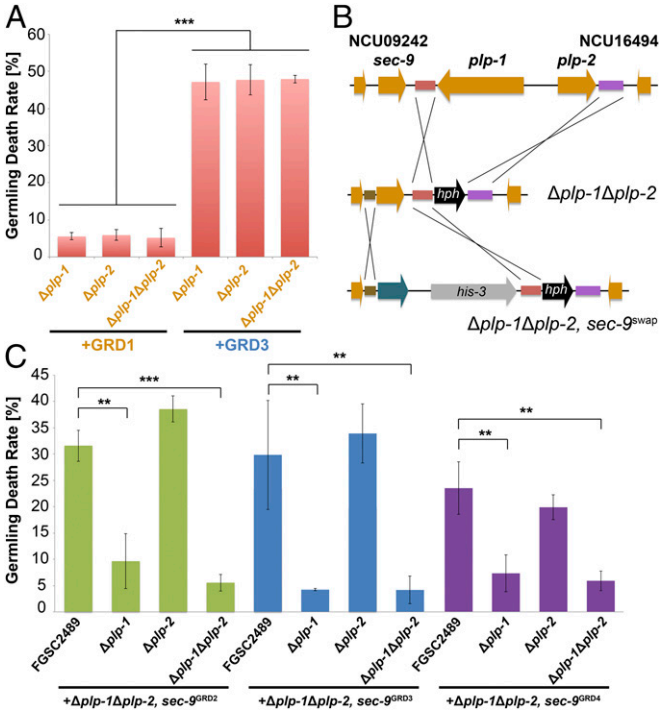

Fig. 3. Genetic interaction of *sec-9* and *plp-1* mediates GRD. (*A*) Germling death frequencies of *Δplp-1*, *Δplp-2* and *Δplp-1 Δplp-2* cells after fusion with their GRD1 (FGSC 2489) parental strain or with a GRD3 (segregant 2) strain. Germling death rates were determined using flow cytometry. Experiments were performed at least in triplicate, with 20,000 events counted per experiment. ***$P < 0.001$, Student's *t* test. (*B*) Strategy for creating *Δplp-1 Δplp-2* and *Δplp-1 Δplp-2*, *sec-9*^{swap} strains by homologous recombination. (*C*) Germling death frequencies of *Δplp-1 Δplp-2*, *sec-9*^{swap} strains (colors correspond to GRDH of the *sec-9* swap) with FGSC 2489, *Δplp-1*, *Δplp-2*, and *Δplp-1 Δplp-2* strains (all GRD1 background). Germling death frequencies were determined using flow cytometry. Experiments were performed at least in triplicate, with 20,000 events counted per experiment. **$P < 0.01$ and ***$P < 0.001$, Student's *t* test.

(~15%) (Fig. S3*A*). Notably, the phylogeny of *sec-9*/*plp-1* showed that GRDH3 is more similar to GRDH4 than to GRDH1 or GRDH2 (Table S1).

Not all nonallelic *sec-9*/*plp-1* interactions induced GRD (Fig. S3 *B*–*E*). For example, an engineered strain carrying the duplicated *plp-1* gene (*Δplp-1 Δplp-2*, *sec-9*^{GRD2} *plp-1.1*^{GRD2}) showed low death frequencies when paired with all *sec-9* swap strains (i.e., nonallelic interaction of *plp-1.1*^{GRD2} and *sec-9* does not mediate GRD) (Fig. S3*C*). However, pairings of a *sec-9*^{GRD2} strain carrying the second *plp-1* gene (*Δplp-1 Δplp-2*, *sec-9*^{GRD2} *plp-1.2*^{GRD2}) showed high death frequency when paired with *sec-9*^{GRD3} *Δplp-1 Δplp-2* or *sec-9*^{GRD4} *Δplp-1 Δplp-2* germlings, but low death frequency in pairings with *sec-9*^{GRD1} *Δplp-1 Δplp-2* (i.e., nonallelic interactions of *plp-1.2*^{GRD2} with *sec-9*^{GRD3} and *sec-9*^{GRD4} mediate GRD) (Fig. S3*C*). These data show that several specific nonallelic *sec-9*/*plp-1* interactions induce GRD, while other nonallelic *sec-9*/*plp-1* interactions have no effect. However, because one incompatible *sec-9*/*plp-1* pair is sufficient to induce GRD, no viable heterokaryons will form between wild isolates of different GRDHs. A potential increase of death frequencies in the presence of several paralogous *plp-1* genes cannot be excluded.

SNARE Domains of SEC-9 Mediate Allelic Specificity. SNARE proteins like SEC-9 are involved in fusion of vesicles with their target membranes; the SNARE domains are essential for formation of the coiled-coil structure with interaction partners syntaxin (Sso1p) and synaptobrevin (Snc1p) (28). Consistent with its potential function as a SNARE protein, GFP-tagged SEC-9 localized as a crescent at the germling tip (Fig. 2*C* and Fig. S2*F*). The N terminus of SEC-9 (first 174 aa) was fairly conserved within the different GRD specificity groups and contained only a few amino acid substitutions that track with GRDH. In contrast, the C-terminal region of SEC-9, which includes the SNARE domains essential for protein function, was highly diverse between the different GRD groups (Fig. 4 *A* and *B*). A sliding window analysis of divergence between *sec-9* sequences from distinct haplogroups confirmed that divergence was higher around the coiled-coil domains (amino acids positions ~200–300) (Fig. S3*F*). To delineate the region of SEC-9 that confers allelic specificity, SEC-9 chimeras were constructed that consisted of the N terminus of SEC-9 from a GRD3 strain fused to the C terminus of SEC-9 from a GRD1 strain, or vice versa; chimeras replaced the *sec-9*^{GRD1} allele in a *Δplp-1 Δplp*-2 strain (Fig. 3*B*). A strain expressing the SEC-9 chimera with the GRD3 N terminus and a GRD1 C terminus showed high death frequencies (~45%) when paired with a GRD3 strain. A strain expressing a SEC-9 chimera with the GRD3 C terminus showed high death frequencies (~35%) when paired with a GRD1 strain (Fig. 4*C*). These data indicated that the C terminus, which includes the SNARE domains of SEC-9, mediates GRD allelic specificity.

To determine whether the SNARE domains alone were sufficient for recognition, we expressed isolated SNARE domains of SEC-9^{GRD3} (SNARE1: amino acids 191 to 257 or SNARE2: amino acids 360 to 422) in a *sec-9*^{GRD1} *Δplp-1 Δplp*-2 strain. We then assessed cell death frequencies when these strains were paired with a GRD1 strain (Fig. 4*D*). The vacuolization phenotype of GRD in fused germlings was assessed, as other GRD-related phenotypes were weaker than with full-length SEC-9. Vacuolization rates were low (~3%) in self-pairings between *sec-9*^{GRD1} *Δplp-1 Δplp-2* (*SNARE1*$^{sec-9\ GRD3}$) germlings or between *sec-9*^{GRD1} *Δplp-1 Δplp-2* (*SNARE2*$^{sec-9\ GRD3}$) germlings (absence of PLP-1) (Fig. 4*D*). However, in pairings between *sec-9*^{GRD1} *Δplp-1 Δplp*-2 (*SNARE1*$^{sec-9\ GRD3}$) or *sec-9*^{GRD1} *Δplp-1 Δplp*-2 (*SNARE2*$^{sec-9\ GRD3}$) and a GRD1 strain (PLP-1 present), high vacuolization rates were observed in fused germling pairs (~30%) (Fig. 4*D*). These data indicated that either of the highly polymorphic SNARE1 and SNARE2 domains of SEC-9 mediates allelic specificity and was sufficient to induce GRD.

In *S. cerevisiae*, Sec9p physically interacts with Sso1/2p and Snc1/2p (28). Surprisingly, unlike *sec-9*, no polymorphisms that result in GRDH-specific amino acid substitutions were present in *sso-1* (NCU02460) or *snc-2* (NCU00566) alleles in the *N. crassa* population (Table S1). Thus, SEC-9 proteins from the four different haplogroups function with identical SSO-1 and SNC-2 proteins for SNARE assembly and vesicle trafficking, a hypothesis supported by the fact that the *sec-9* swap mutants were viable.

To assess the correlation of diverse SEC-9 protein interactions with conserved SSO-1 and SNC-1 homologs, the level of amino acid polymorphism and divergence at SNARE domains of SEC-9 across three fungal species (*N. crassa*, *P. anserina*, and *C. parasitica*) was determined. Amino acid variants were mapped onto a predicted structure of the SNARE domains obtained by homology modeling onto Sec9p. Nearly the entire exposed surface of the SNARE domains showed extreme levels of variation. A reduced level of variation was only detected in a few positions predicted to form the interface with SSO-1 and SNC-1 homologs (Fig. 4*E*). This conservation of essential amino acids in SEC-9 that are associated with interactions with SSO-1 and SNC-1 homologs is consistent with the conserved essential function of SEC-9, despite general sequence diversity in filamentous fungal species.

PLP-1 Is a Fungal NLR. The data presented above show that GRD is a regulated process that depends on nonallelic interactions between *sec-9* and *plp-1*. PLP-1 has the tripartite domain architecture of an NLR (Fig. 5*A*). In contrast, PLP-2 is missing an NBD. Cellular localization studies using functional C-terminal–tagged proteins (GFP and mCherry) showed that both PLP-1 and PLP-2 localize to the periphery of the cell (Fig. 2*C* and Fig. S2*G*). Protein and nucleotide alignments of PLP-1 from the 23 sequenced wild isolates indicated that the patatin-like domain

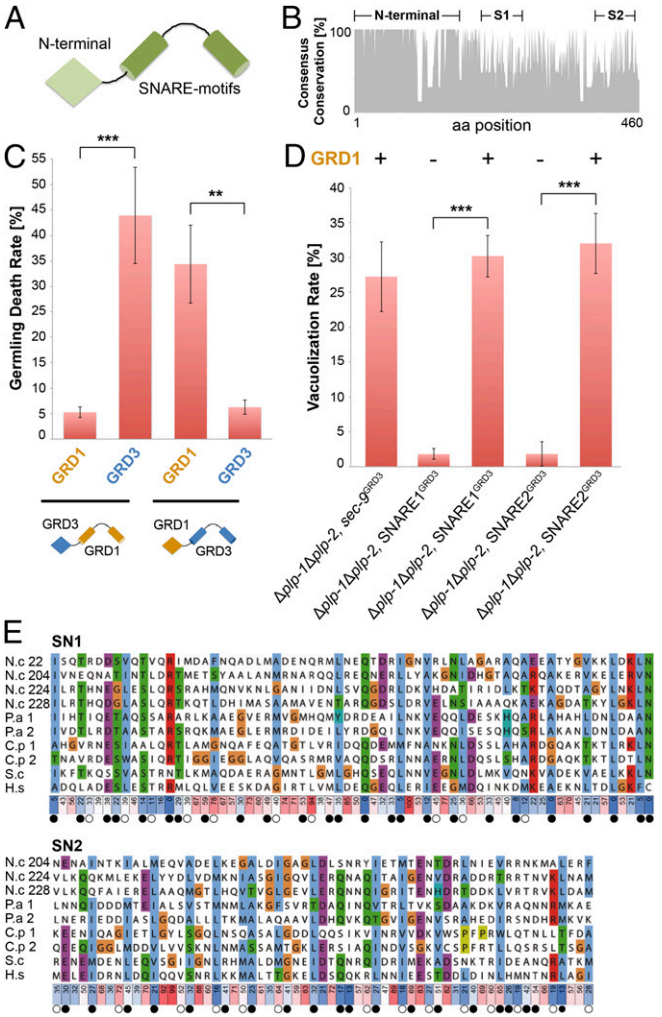

Fig. 4. Polymorphic SNARE motifs of SEC-9 are recognized by PLP-1 during GRD. (*A*) Schematic presentation of SEC-9 of *N. crassa*. SEC-9 has an N-terminal extension and two C-terminal SNARE motifs. (*B*) Consensus sequence conservation of SEC-9 within 23 wild isolates of an *N. crassa* population along every amino acid position. Note the higher conservation within the N-terminal region. (*C*) Germling death frequencies of *Δplp-1 Δplp-2*, *sec-9*^{chimera1} (*Left* two columns; chimera pictured below) and *Δplp-1 Δplp-2*, *sec-9*^{chimera1} (*Right* two columns; chimera pictured below) in pairings with GRD1 (FGSC 2489) or GRD3 (segregant 2) germling. Colors correspond to the respective GRDH (yellow, GRDH1; blue, GRDH3). Death rates were measured by flow cytometry. Experiments were performed at least in triplicate, with 20,000 events counted per experiment. $^{**}P < 0.01$ and $^{***}P < 0.001$, Student's *t* test. (*D*) Vacuolization frequency of *Δplp-1 Δplp-2*, SNARE1^{GRD3} or *Δplp-1 Δplp-2*, SNARE2^{GRD3} germlings undergoing self-fusion (columns 2 and 4) or when paired with GRD1 germlings (FGSC 2489). The *Δplp-1 Δplp-2*, *sec-9*^{GRD3} strain served as a positive control. Vacuolization rates were determined by microscopy. Experiments were performed in triplicate, with at least 350 germlings evaluated per experiment. $^{***}P < 0.001$, Student's *t* test. (*E*) Alignment of the SN1 and SN2 SNARE regions of the SEC-9 homologs from *N. crassa* wild isolates (N.c), *Podospora anserina* (P.a), and *Cryphonectria parasitica* (C.a) with SNARE domains of yeast SEC9 (S. c.) and human SNAP25 (H.s), using ClustalOmega. For the *N. crassa*, *P. anserina* and *C. parasitica* sequences, for each site, the average of all intraspecific pairwise alignment scores (extracted from Jalview) were calculated and then normalized to set the most divergent site to 100 (red) and the most conserved site (no intraspecific polymorphism) to 0 (blue). For *N. crassa* in SN2, only three of the four allelic types were used, as the JW22 sequence could not unambiguously be aligned without gaps. Black dots indicate interfaces with SS0-1/SNC-2, and empty dots indicate self-interface (SEC-9 SNARE1 with SNARE2).

and the NBD domain showed some conserved motifs, both within and between GRDHs (Fig. S3 *G–I*). Sequence divergence was more heterogeneous and diversity was higher along the TPR helical domain (Fig. S3 *H* and *I*).

Patatin-like domains have a conserved GGxR/K motif and a catalytic dyad formed by a serine and aspartic acid residue (29). The GGxR/K motif is conserved in PLP-1, and the predicted catalytic dyad is formed by serine 64 and aspartic acid 204 (Fig. 5*B*). In the NBD domain of PLP-1, the Walker A motif (GxxGxGKS/T), which is required for nucleotide binding, and the Walker B motif (xLhhhD), which is required for nucleotide hydrolysis, are conserved (Fig. 5*C*).

To test the hypothesis that the phospholipase catalytic activity and NBD motifs identified in PLP-1 are essential for GRD function, we generated four point mutations affecting either of the two residues of the catalytic dyad of the patatin-like domain (S64A or D204A) and the P-loop motif (Walker A; K414A), or the Walker B motif (D484A) of the NBD domain (Fig. 5 *B* and *C*). These constructs were introduced into the *sec-9*^{GRD1} *Δplp-1 Δplp-2* strain. The mutated proteins retained their native localization to the periphery of the cell (Fig. 5*D*). However, the activity of these proteins in mediating GRD was strongly affected (Fig. 5*E*). The *sec-9*^{GRD1} *Δplp-1 Δplp-2* strain expressing GFP-tagged wild-type PLP-1 showed high death rates (~30%) when paired with a *sec-9*^{GRD3} *Δplp-1 Δplp-2* strain, but the *sec-9*^{GRD1} *Δplp-1 Δplp-2* strains expressing PLP-1^{S64A}, PLP-1^{D204A}, or PLP-1^{K414A} mutations showed low death rates (~5%). The *sec-9*^{GRD1} *Δplp-1 Δplp-2* strains expressing PLP-1^{D484A} (Walker B motif mutation) still induced some death (~15%) when paired with a *sec-9*^{GRD3} *Δplp-1 Δplp-2* strain. These data indicated that PLP-1 requires functional patatin-like phospholipase activity and a functional NBD for full GRD function.

Physical Interaction of Incompatible SEC-9 and PLP-1 Induces PLP-1/PLP-2 Complex Formation. Studies of NLRs in other organisms have suggested a model where ligand recognition results in a conformational change that relieves autoinhibitory intramolecular interactions, allowing NOD domain-dependent nucleotide binding and oligomerization, which, in turn, activates downstream reactions (30). To examine if PLP-1 functions similar to other NLRs, we performed co-IP experiments to test physical interactions between SEC-9, PLP-1, and/or PLP-2 by creating strains that expressed differentially tagged PLP-1, PLP-2, and SEC-9 proteins (GFP/mCherry). We first assessed self-assembly of PLP-1^{GRD1}, self-assembly of PLP-2^{GRD1}, and interaction between PLP-1^{GRD1} and PLP-2^{GRD1} in the absence of GRD; no interaction was detected (Fig. 6*A*). To assess interactions between PLP-1^{GRD1} and PLP-2^{GRD1} after GRD induction, GRD1 germlings expressing the tagged proteins were paired with a GRD3 strain. Self-assembly of PLP-1^{GRD1} and interaction of PLP-1^{GRD1} with PLP-2^{GRD1} were detected (Fig. 6*B* and Fig. S4*A*). However, interactions between SEC-9^{GRD1} with either PLP-1^{GRD1} or PLP-2^{GRD1} were not detectable independent of GRD induction (Fig. 6*C* and Fig. S4*B*). These data indicated that physical interaction/oligomerization of PLP-1 and PLP-2 of identical GRD specificity occurred under conditions of GRD, but not between SEC-9 and PLP-1/PLP-2 of identical GRD specificity.

Since nonallelic genetic interactions between *sec-9* and *plp-1* induced GRD (Fig. 3), we hypothesized that molecular recognition occurs via a physical interaction when SEC-9 and PLP-1 are of different GRD specificity. To test this hypothesis, we created GFP-labeled SEC-9^{GRD3} constructs driven by the *tef-1* promoter (high constitutive expression) or driven by the native *sec-9* promoter. Co-IP experiments were performed on strains expressing GFP-labeled SEC-9^{GRD3} paired with strains expressing mCherry-labeled PLP-1^{GRD1} or PLP-2^{GRD1}. Importantly, PLP-1^{GRD1} and SEC-9^{GRD3} coimmunoprecipitated, while an interaction between PLP-2^{GRD1} and SEC-9^{GRD3} was not detectable (Fig. 6*C* and Fig. S4*B*). These data indicated that SEC-9 and PLP-1 of different GRD

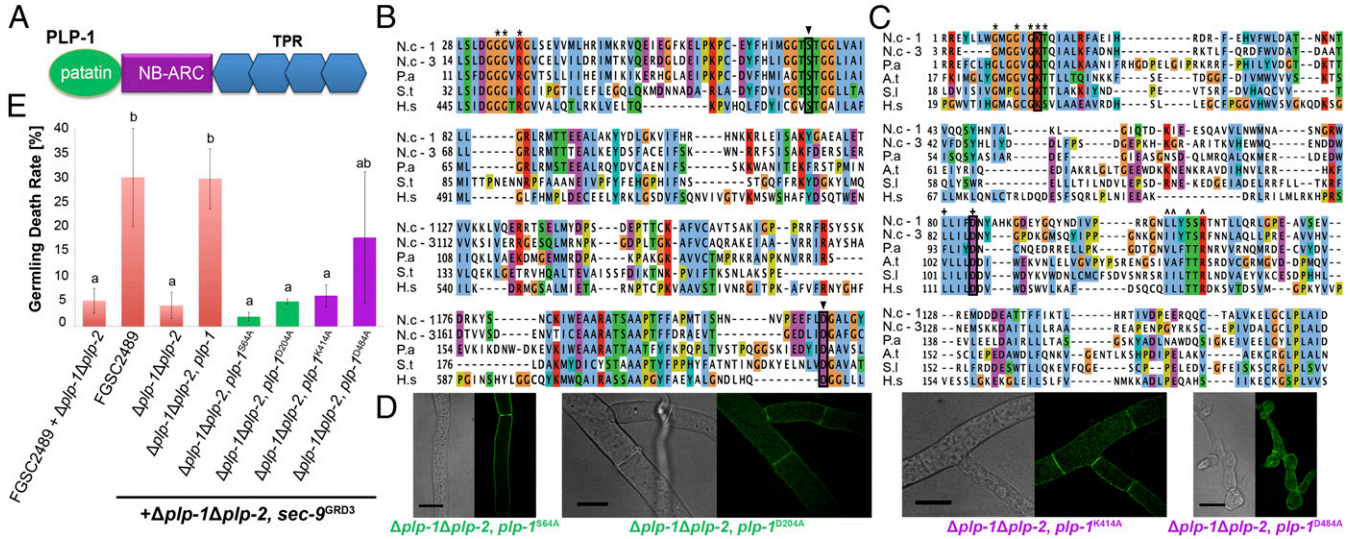

Fig. 5. Patatin-like domain and NBD of PLP-1 are essential for GRD. (*A*) Schematic presentation of PLP-1. PLP-1 has a tripartite domain architecture with an N-terminal domain (patatin-like), a central NBD, and C-terminal TPRs. (*B*) Alignment of patatin-like phospholipase domains of PLP-1^{GRD1} and PLP-1^{GRD3} of *N. crassa* (N.c), PaPLP1-1 of *P. anserina* (P.a), patatin from potato (S.t), and human iPLA2 (H.s). The GGxR/K motif (*) and the catalytic dyad formed by a serine and aspartic acid (▼) are conserved. Essential amino acids that have been mutated to alanine in PLP-1 are circled. (*C*) Alignment of NBD domains of PLP-1^{GRD1} and PLP-1^{GRD3} of N.c, PaPLP1-1 of P.a, DRL24 of *Arabidopsis thaliana* (A.t), tomato K4BY49 (S.l), and human APAF1 (H.s). The Walker A motif (*), the Walker B motif (+), and the nucleotide sensor 1 (^) residues are conserved. Essential amino acids that have been mutated to alanine in PLP-1 are circled. (*D*) Localization of PLP-1 is not affected by mutations introduced in the patatin-like domain (S63A, D204A; green) or in the NB-ARC domain (K414A, D484A; purple). (Scale bars: 10 μm.) (*E*) Germling death frequencies are reduced when GRD1 strains expressing PLP-1 with mutations in the patatin-like domain and in the NB-ARC domain are paired with a strain expressing SEC-9^{GRD3}. Colors correspond to the domain affected by the mutations (red, control strains; green, patatin-like; purple, NB-ARC). Germling death frequencies were determined using flow cytometry. Experiments were performed at least in triplicate, with 20,000 events counted per experiment. Different letters (a, b) denote a statistically significant difference. $P < 0.05$, one-way ANOVA with post hoc Tukey honest significant difference test.

specificity physically interact during the GRD reaction, while SEC-9 and PLP-2 do not.

While the patatin-like domain, as well as the NB-ARC domain, of PLP-1 is necessary for GRD (Fig. 5*E*), it was unclear if the oligomerization of PLP-1/PLP-2 proteins is necessary and sufficient for GRD. We reasoned that mutations introduced in these domains that prevented GRD may also abolish protein/protein interactions. To test this hypothesis, strains expressing mutated versions of GFP- and mCherry-labeled PLP-1 [mutations in the catalytic dyad of the patatin-like domain (S64A or D204A) or NBD mutations in the P-loop motif (K414A) or Walker B motif (D484A)] were paired with a *sec-9*^{GRD3} *Δplp-1 Δplp-2* strain. Co-IP experiments showed that mutations in the NBD domain (K414A or D484A) prevented the self-association of PLP-1 proteins (Fig. 6*D* and Fig. S4*C*). In contrast, mutations in the patatin-like domain (S64A or D204A) did not affect self-association of PLP-1 (Fig. 6*D* and Fig. S4*C*), even though these mutations completely eliminated GRD (Fig. 5*E*). These data indicated that self-association of PLP-1 via the NB-ARC domain is not sufficient for GRD. Instead, a functional patatin-like domain is essential to transmit the GRD signal.

We reasoned that SEC-9^{GRD3} might interact with PLP-1^{GRD1} containing mutations in the NB-ARC domain or in the patatin-like domain, despite the lack of GRD. To test this hypothesis, we cocultivated strains expressing mutated versions of mCherry-labeled PLP-1^{GRD1} (S64A or K414A) with a *Δplp-1 Δplp-2* strain expressing SEC-9^{GRD3}–GFP. In co-IP experiments, a strong interaction between SEC-9^{GRD3} and PLP-1^{S64A} (catalytic dyad mutation) was observed, while a weak interaction between SEC-9^{GRD3} and PLP-1^{K414A} (Walker A motif mutation) was detected (Fig. 6*C*). These data support the hypothesis that recognition of SEC-9 by PLP-1 is not affected by mutations in the NBD or the patatin-like domains. A weak interaction of SEC-9^{GRD3} with PLP-1^{K414A} could be explained by the lack of signal enhancement due to the lack of PLP-1^{K414A} self-association. Together, these data indicated that the interaction between SEC-9 and PLP-1 of different GRD specificity is independent of NBD function and patatin-like activity, and occurs even in the absence of GRD.

***sec-9* and *plp-1* Homologs Determine *het-z* HI in *P. anserina*.** In *C. parasitica*, orthologs of *plp-1* and *sec-9* are associated with HI mediated by allelic differences at the *vic2* locus (21). In a systematic search for molecular components of *het* loci in other fungi, we determined that *sec-9/plp-1* orthologs mediate *het-z* incompatibility in *P. anserina* (Fig. S5*A*). The *Het-z* locus is one of nine HI loci of *P. anserina*, with two allelic specificities, *het-z1* and *het-z2*, defining the incompatibility system. If strains of different *het-z* specificity fuse, they show characteristic cell death reactions and barrage formation at the contact point between incompatible colonies (Fig. S5*A*). Incompatibility of *het-z* was assessed via transformation efficiency tests [i.e., transformation efficiency was reduced when *PaSec9*$^{het\text{-}z1}$ (*PaSec9-1; Pa_1_11410*) was transformed into a *het-z2* background strain or when *PaSec9*$^{het\text{-}z2}$ (*PaSec9-2*) was transformed into a *het-z1* background strain] (Fig. S5*B*). Likewise, the introduction of *PaPlp1* (*plp-1* ortholog: *Pa_1_11380*) from *het-z1* strains (*PaPlp1-1*) reduced transformation efficiencies in *het-z2* strains, while the introduction of *PaPlp1-2* reduced transformation efficiencies in *het-z1* strains (Fig. S5*B*). As in *N. crassa*, high levels of allelic diversity were detected for *PaSec9* and *PaPlp1* in *het-z1* and *het-z2* strains (Figs. S5*D* and S6).

PaSec9 is also an essential gene in *P. anserina*, as homokaryotic Δ*PaSec9* strains could not be recovered. To test the role of *PaPlp1* in defining *het-z* incompatibility, *PaPlp1* was inactivated in both *het-z1* and *het-z2* backgrounds. The *ΔPaPlp1-1* and *ΔPaPlp1-2* strains retained incompatibility to *het-z2* and *het-z1* strains, respectively, but were fully compatible with each other (Fig. S5*A* and Table S3). The *ΔPaPlp1-1* strains transformed with *PaSec9-2* acquired incompatibility to *het-z1*, and the *ΔPaPlp1-2* strains transformed with *PaSec9-1* acquired incompatibility to *het-z2* (Fig. S5*A* and Table S3). *PaSec9-2* did not lead to a reduction in transformation efficiency when introduced into *ΔPaPlp1-1* (Fig. S5*B*). Collectively, these data confirmed that *PaPlp1* and

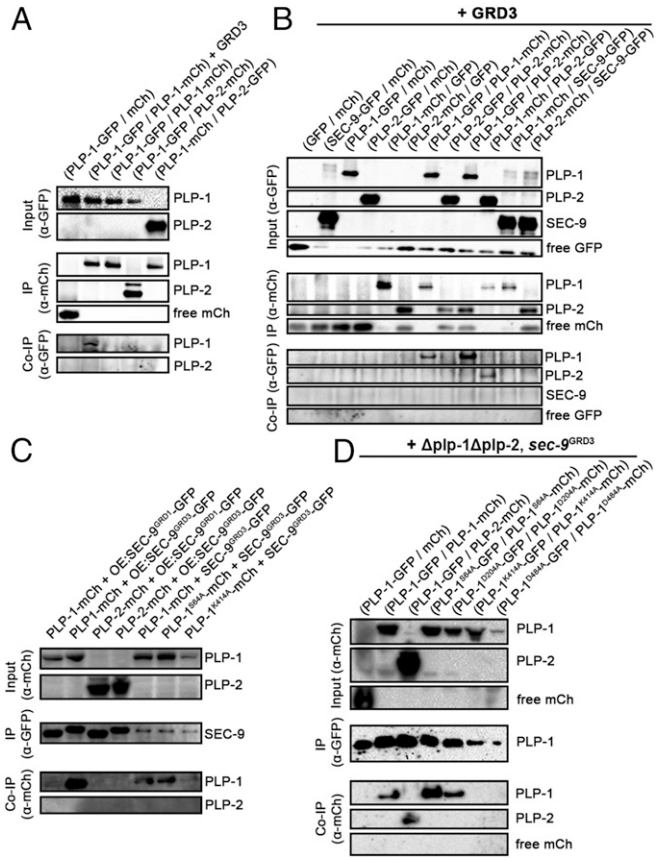

Fig. 6. Interaction studies by co-IP experiments. Input panels show Western blots of total protein extracts isolated from 6-h-old germlings probed with either anti-GFP antibodies (*A* and *B*) or anti-mCherry (mCh) antibodies (*C* and *D*). Immunoprecipitation (IP) panels show anti-mCh–immunoprecipitated (*A* and *B*) or anti-GFP–immunoprecipitated (*C* and *D*) proteins probed with anti-mCh (*A* and *B*) or anti-GFP (*C* and *D*) antibodies. Co-IP panels show anti-mCh–immunoprecipitated (*A* and *B*) or anti-GFP–immunoprecipitated (*C* and *D*) proteins probed with anti-GFP (*A* and *B*) or anti-mCh (*C* and *D*) antibodies. Parentheses indicate tagged proteins that are expressed in one heterokaryotic strain. (*A*) Heterokaryotic germlings expressing various combinations of tagged GRD1 proteins were cultivated. GRD was triggered by cocultivation of a heterokaryotic strain (PLP-1–GFP/PLP-1–mCh) with a GRD3 strain (lane 2). (*B*) Heterokaryotic germlings expressing various combinations of tagged GRD1 proteins were cocultivated with germlings of GRD3 specificity to induce GRD. (*C*) Germlings expressing tagged proteins as indicated were cocultivated to induce germling fusion between the strains. During cultivation, GRD occurred if wild-type PLP-1 interacted with SEC-9^{GRD3} (lanes 2, 4, and 5). Tagged SEC-9 was expressed in addition to endogenous SEC-9^{GRD1}, and was either overexpressed by the *tef-1* promoter (OE) or controlled by the native *sec-9* promoter (lanes 5–7). Note that there is a size difference between SEC-9^{GRD1} (43.5 kDa) and SEC-9^{GRD3} (47 kDa). (*D*) Heterokaryotic germlings expressing various combinations of tagged GRD1 proteins were cocultivated with germlings of a *Δplp-1 Δplp-2, sec-9*^{GRD3} strain. During cultivation, GRD occurred if wild-type PLP-1 interacted with SEC-9^{GRD3} (lanes 1–3), while in combinations with mutated PLP-1, no GRD occurred (S64A, D204A, and K414A) or GRD was reduced (D484A) (compare Fig. 5*E*). PLP-1–GFP, ∼175 kDa; PLP-2–GFP, ∼90 kDa; SEC-9–GFP, ∼70 kDa; GFP, ∼25 kDa; mCh, ∼30 kDa. Reciprocal co-IP panels are shown in Fig. S4.

PaSec9 determine *het-z* incompatibility through nonallelic interaction between incompatible *PaPlp1* and *PaSec9* alleles (Fig. S5*C*). Hence, the *het-z* locus of *P. anserina* acts analogous to the *sec-9*/*plp-1* locus of *N. crassa*.

As shown for *N. crassa*, amino acid differences between PaPLP1-1 and PaPLP1-2 were mainly located in the TPR region (Fig. S6 *B* and *C*). Chimeric constructs in which the TPR domains were exchanged between *PaPlp1-1* and *PaPlp1-2* were introduced into *ΔPaPlp1-1* strains; the TPR domains mediated *het-z1* and *het-z2* allelic specificity (Tables S3 and S4). To analyze if the patatin-like domain and the NB-ARC domain have the same essential function in PaPLP1 as in *N. crassa* PLP-1, point mutations were introduced in both domains. The two amino acids forming the catalytic dyad of the predicted patatin-like domain (S57A and D202A) and the P-loop of the NBD (K415R) of *PaPlp1-2* were mutated. Neither mutant allele reduced transformation efficiencies when introduced into *het-z1* strains. *ΔPaPlp1* strains expressing the mutant alleles were compatible with both a *ΔPaPlp1-1* strain and a *ΔPaPlp1-2* strain. (Fig. S5*E* and Table S3). These data indicated that both the phospholipase activity and NBD of PaPLP1 are essential for conferring HI in *P. anserina*.

As reported above for SEC-9 of *N. crassa*, amino acid differences between *PaSec9* allele products were mainly located in the region encoding the SNARE domains (Fig. S6*A*). Chimeric constructs between *PaSec9-1* and *PaSec9-2* confirmed that the SNARE domains mediate *het-z1* and *het-z2* specificity (Table S3). These data indicate that the regions of elevated variability (SNARE domain of SEC-9 and TPR domain of PLP-1) determine allelic specificity.

Convergent Evolution Is the Most Strongly Supported Scenario for the Common Use of the *plp-1*/*sec-9* System in Allorecognition in Three Fungal Genera. The finding that three different fungal genera use the *plp-1*/*sec-9* system in allorecognition can be explained by an independent, de novo recruitment of the same genetic system for functioning in allorecognition (i.e., convergent evolution) or by the fact that this allorecognition genetic system was already in use in the common ancestor of these three species, and that ancient allelic lineages have been maintained by balancing selection over long evolutionary time scales (31) (i.e., TSP, the retention of ancient allelic lineages through speciation events). To distinguish between these two hypotheses, we aligned *sec-9* and *plp-1* sequences from the three genera *Neurospora*, *Podospora*, and *Cryphonectria* and carried out phylogenetic inference using maximum likelihood approaches. Gene genealogies revealed that the TSP detected in *N. crassa* and *N. discreta* does not extend beyond this genus. Instead, when comparing *Neurospora*, *Podospora*, and *Cryphonectria*, different allele types of *sec-9* and *plp-1* homologs grouped by species (Fig. S6*C*). These data suggest that the common use of the *plp-1*/*sec-9* system in allorecognition in three divergent genera of filamentous ascomycete species is the result of convergent evolution.

Discussion

Recognition of nonself is typically dichotomized into allo- and xenorecognition, depending on whether conspecific or heterospecific (typically pathogenic) nonself is being detected (32). Allorecognition mechanisms play an important role in various aspects of multicellular life. For example, in flowering plants, self-incompatibility is a pollen recognition system that avoids inbreeding caused by self-pollination and requires coevolution among several interacting components within the S-locus (33, 34). In basal metazoans, allorecognition responses mediate rejection between unrelated colonies and, similar to fungal HI, are controlled by highly variable genetic systems (35). Xenorecognition processes, in turn, are typically exemplified by responses to pathogen attack or establishment of mutualistic symbiotic interactions. Our data indicate that NLRs can be involved in both aspects of nonself recognition.

Although recent research has revealed that the repertoire of NLR-like genes in fungal genomes is quite large and variable (10), functional studies of these NLR-like genes are limited. One reason is the lack of tractable fungal pathogen systems to dissect fungal NLR-dependent immunity. However, fungal allorecognition systems, which may have evolved through exaptation similar to hybrid necrosis in plants (13), can be used to study the origin and functioning of fungal innate immunity. The fungal NLR-like protein PLP-1 induces allorecognition and PCD in the three distinct filamentous fungal species *N. crassa*, *P. anserina*, and *C. parasitica* (this study and ref. 21). PLP-1 has a tripartite architecture characteristic for NLRs with a central NBD, an N-terminal patatin-like domain,

and C-terminal TPRs. Cell death induction was dependent on both the patatin-like domain and NBD. PLP-1 interacts with the SNARE protein SEC-9; the SNARE domains were necessary and sufficient to confer allorecognition and cell death.

Our data support a model whereby PCD is induced if TPR domains of PLP-1 detect SNARE domains of incompatible SEC-9 proteins (Fig. 7). Upon physical interaction with incompatible SEC-9 proteins, PLP-1 is activated and oligomerizes into a complex that involves other proteins (shown here for PLP-2). PLP-1/SEC-9 allorecognition-related cell death is dependent on the lipase activity of the patatin-like domain. The finding that the N-terminal domain of PLP-1 has enzymatic activity essential for HI constitutes a unique role of NLRs, as other characterized N-terminal domains of animal and plant NLRs act as adaptors that perform signaling functions (36). Interestingly, patatin-like domains have been reported to play a role in host-defense–related PCD in plants (37, 38). PLP-1–induced cell death could be a direct consequence of alteration of membrane phospholipids via the patatin-like phospholipase domain. In this case, the PLP-1 complex might act as a membrane toxin itself. Alternatively, PLP-1 activity might rely on production of a secondary messenger and downstream signaling that activates executioners of cell death. Oligomerization has been shown for metazoan NLRs (15), and, in plants, it has recently been shown that the NLR RPM1 requires self-association to be functional (39). PLP-1 also self-associates, and oligomerization of PLP-1 was NBD-dependent. However, because proteins without functional NBD (PLP-2) interact with PLP-1 during GRD, other domains must contribute to protein oligomerization once PLP-1 is activated.

It has been proposed that the allorecognition function of fungal NLRs is derived by exaptation from a function in pathogen defense (11). Based on the guard model for NLR function in plants (3), fungal NLRs would survey integrity of key cellular components and trigger an immune response if pathogen effectors compromise the structure of these components. The guard model for plants assumes that a response is elicited when a pathogen effector disrupts a complex between the guardee (a host protein) and the guard (an NLR) (12). In our model, the guarding occurs indirectly, as an interaction between the compatible guardee (SEC-9) and its guard (PLP-1) was not detected. Therefore, instead of disrupting a complex between the guardee and the guard, in this system, a complex is formed between the guard and the modified/nonself guardee, which initiates downstream reactions resulting in cell death. Considering the essential role of SEC-9 in exocytosis and autophagy (40), the SNARE complex might also constitute a relevant cellular target for pathogen effectors. In fact, pathogenic microorganisms use the SNARE motif to manipulate host membrane fusion (41). For example, *Legionella* and *Chlamydia* effectors directly target membrane fusion by SNARE mimicry and interactions with host SNARE proteins to create intracellular compartments (42–44). In plants, the exocyst, which includes SNARE proteins, was found to be targeted by effectors of fungal or oomycete pathogens (45–47).

The level of intraspecific polymorphism in SEC-9 proteins from *N. crassa*, *P. anserina*, and *C. parasitica* is extreme, especially in the SNARE domains essential for function. This functionally critical region of the protein also defines allorecognition specificity. We hypothesize that the coiled-coil SNARE domains, which are essential for vesicle fusion, have been targeted by selection in an arms race with effectors aimed at inactivating exocytosis/autophagy, resulting in rapid diversification of *sec-9*. The guard model for NLR function implies that protection for SEC-9 could be under the surveillance of PLP-1–like NLRs. If a pathogen targets or mimics the SEC-9 SNARE complex, the PLP-1 NLR is activated and cell death is induced. Once established, such a two-component guard/guardee system could be coopted by exaptation into an allorecognition system, as genetic variants of the guardee are specifically recognized by the NLR guard.

This report shows that the same gene pair behaves as an allorecognition locus in three distantly related fungal genera (*Neurospora*, *Podospora*, and *Cryphonectria*). Other *het* genes identified in these species either showed no clear orthologs or were not polymorphic. The common role for the PLP-1 (vic2)/SEC-9 pair in allorecognition suggests long-term conservation of the derived allorecognition function. The lack of transspecies retention of ancient allelic lineages suggests that this gene pair has been repeatedly recruited as an allorecognition system in filamentous fungi. This allorecognition system stands out among fungal recognition systems by its common role in multiple divergent species and stresses the important role of surveillance of the essential SEC-9 SNARE in fungi. The involvement of PLP-1 in allorecognition makes this system especially tractable to study general NLR functions at the molecular level. In future studies, it will be important to elucidate the exact mechanism by which PLP-1 activation induces cell death and to identify downstream contributors of the death-inducing complex. SEC-9/PLP-1 provides a powerful system for comparative analyses across biological kingdoms on the structural and molecular function of allorecognition, NLR function, and downstream processes that can induce different cellular outcomes, including death.

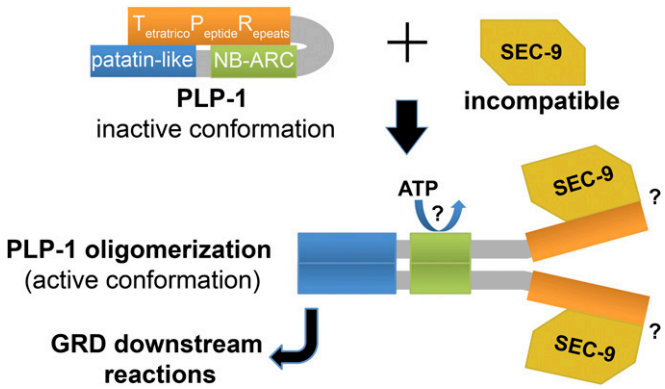

Fig. 7. Model for NLR function of PLP-1. Our data suggest that PLP-1 functions as a fungal NLR that seems to act in a similar way to plant and animal NLRs. Our model states that PLP-1 is kept in an inactive conformation when not induced. Interaction with SEC-9 of different GRD specificity activates PLP-1. Recognition is predicted to occur via the TPR domain and the SEC-9 SNARE domains, as these regions confer allelic specificity. The involvement of other proteins cannot be excluded. Activation of PLP-1 induces oligomerization of PLP-1, which requires a functional NB-ARC domain. Once initiated, proteins without a functional NB-ARC domain can participate in the GRD complex (PLP-2). The GRD signal for cell death is transmitted via the N-terminal patatin-like phospholipase activity.

Materials and Methods

Strain Construction and Growth Conditions. Standard protocols for *N. crassa* can be found on the *Neurospora* homepage at the FGSC (www.fgsc.net/Neurospora/NeurosporaProtocolGuide.htm). Strains were grown on Vogel's minimal medium (VMM) (48) (with supplements as required) or on Westergaard's synthetic cross-medium for mating (49).

The wild *N. crassa* strains used in this study were isolated from Louisiana and are available at the FGSC (17, 18, 24). FGSC 2489 served as the parental strain for gene deletions and as a WT control for all experiments, unless stated otherwise. Single-deletion mutants are available at the FGSC (50, 51). Genotyping of the *Δsec-9* mutants deposited at the *Neurospora* knockout collection using *sec-9*-specific primers showed that *sec-9* was still present in both mating types. When we recapitulated the knockout by homologous recombination, we were unable to purify homokaryotic hygromycin-resistant ascospores from primary transformants. Therefore, *sec-9* seems to be essential in *N. crassa*. To create the *Δplp-1 Δplp-2* mutant, a deletion construct was created using the method of fusion PCR (52). Fusion PCR was also used to create constructs for swapping *sec-9*^{GRD1} with *sec-9* of different GRD specificity.

The plasmid pMF272 (AY598428) (53) was modified as described by Heller et al. (17) to create *gfp*-fusions to *sec-9*, *plp-1*, and *plp-2* and to express SNARE1 or SNARE2 of *sec-9*^{GRD3} targeted to the *his-3* locus. Site-directed mutagenesis was used to introduce point mutations in the NBA-ARC and patatin-like domains of *plp-1*. The plasmid pTSL88F (includes 432 bp of the

terminator region of NCU00762) is a derivative of the plasmid pTSL84C (54) and was used to create *mCherry* fusions to *plp-1* and *plp-2*. For expressing *plp-1* of different GRDHs in the *Δplp-1 Δplp-2*; *sec-9* swap strains, *plp-1.1* and *plp-1.2*, including their native promoter regions, were amplified from genomic DNA of various wild isolates (JW199, JW258, and JW228) and cloned into the vector pCSR1 (55) using the enzymes PstI, AgeI, or EcoRI (5′), and PacI (3′). All constructs were transformed into the respective *Δplp-1 Δplp-2; sec-9* swap strains with selection for cyclosporin-resistant transformants and then backcrossed for purification with the *Δplp-1 Δplp-2*, *his*$^{-}$ mutant.

Standard methods for growth and manipulation of *P. anserina* were used as described on the *Podospora* Genome project homepage (podospora.i2bc.paris-saclay.fr/methods.php). Barrage assays for defining incompatibility phenotypes were performed on standard D0 medium. The deletion cassettes were then used to transform *PaKu70::ble het-z1* or *het-z2* strains (56). For cloning of the *het-z* locus, six plasmids covering 57 kb of the region of Pa_1_11420 (spanning from Pa_1_11380 to Pa_1_1540) were recovered from a *het-z1* genomic library (a generous gift of Robert Debuchy, CNRS, Orsay, France) and introduced by transformation into the *het-z2* strain. A single plasmid led to reduction in transformation efficiency (GA0AB122CC07) and contained four genes (Pa_1_11410 to Pa_1_11440). Deletion constructs were obtained using NdeI, SmaI, SphI, XbaI, and XhoI, leading to deletion of one or several of the four genes. Only constructs bearing Pa_1_11410 and a construct containing only Pa_1_11410 led to a reduction in transformation efficiency. Mutants of the catalytic site residues of the patatin domain (S57A and D202A) and P-loop (K415R) of the *PaPlp1-2* product were obtained by site-directed mutagenesis. The chimeric alleles of *PaPlp1* with swapped TPR repeats and the chimeric alleles of *PaSec9* with swapped SNARE domains were obtained by fusion PCR. Exchanged fragments spanned positions 1–660 for *PaPlp-1* and positions 1–194 for *PaSec9* (Fig. S6).

Transmission Electron Microscopy Analyses. Transmission electron microscopy preparations (Electron Microscopy Laboratory, University of California, Berkeley) were modified from those used by Fleissner et al. (57). Briefly, 100 mL of liquid VMM was inoculated with conidia of one or two strains at a concentration of 1×10^6 cells per milliliter and incubated at 30 °C for 5 h (shaking at 220 rpm for 2.5 h and standing for 2.5 h). After harvesting by centrifugation, cells were fixed with electron microscopy fix [2% glutaraldehyde, 4% paraformaldehyde, 0.04 M phosphate buffer (pH 7.0)], followed by 2% $KMnO_4$ treatment. Dehydration was achieved through a graded ethanol series before embedding the samples in resin.

Flow Cytometry. Cultivation for flow cytometry experiments was identical to cultivation for microscopic vacuolization assays, but agar was substituted with 20% Pluronic F-127 (Sigma–Aldrich) in VMM plates. After 4.5–6 h of cultivation at 30 °C, plates were put to −20 °C for 10 min to liquefy the medium. Germlings were harvested by centrifugation and washed twice in cold PBS. Germlings were suspended in 1 mL of PBS containing 0.1 μM SYTOX Blue (Life Technologies) and 0.15 μM propidium iodide (Sigma–Aldrich) before analyses on a BD LSR Fortessa X-20 (BD Biosciences). Two vital dyes were used as a technical control. SYTOX Blue fluorescence was detected with a no dichroic 450/50 filter after excitation using a 405-nm laser. Propidium iodide fluorescence was detected with a 685 LP 710/50 filter after excitation using a 488-nm laser. In each run, 20,000 events were recorded. Each experiment was performed at least three times. Ungerminated conidia were used as a negative control in each experiment, and gates were set to exclude conidia from the analysis (Fig. S1). Data were analyzed using the Cytobank Community software (community.cytobank.org/). The germling death rates were shown to correspond to the average rate of fluorescent cells from all experiments. Because results for SYTOX Blue and propidium iodide were not significantly different (Fig. S1), results for propidium iodide are shown throughout the paper.

Microscopic Vacuolization Assays. Vacuolization and cell death occurred later in the strains *Δplp-1Δplp-2* SNARE1$^{sec-9\ GRD3}$ and *Δplp-1Δplp-2* SNARE2$^{sec-9\ GRD3}$. Flow cytometry could not be used to measure GRD for those strains. Instead, vacuolization was quantified microscopically. Conidial suspensions were prepared as described by Heller et al. (17). An aliquot of 45 μL of conidial suspension from two strains was mixed, and 80 μL of this final mixture was spread on VMM agar plates (60 × 15 mm). Plates were incubated for 6.5–7 h at 30 °C before vacuolization assessment. At least six photographs were taken for each experiment, and the percentage of vacuolized germlings in the mixture was determined.

Confocal Microscopy. Cellular localization studies were performed with a Leica SD6000 microscope with a 100×, 1.4-N.A., oil-immersion objective equipped with a Yokogawa CSU-X1 spinning disk head and a 488-nm laser for GFP fluorescence and a 563-nm laser for mCherry fluorescence controlled by Metamorph software (Molecular Devices).

Immunoprecipitations and Western Blotting. Immunoprecipitation preparations were modified from those used by Jonkers et al. (54). One hundred milliliters of liquid VMM was inoculated with conidia of one or two strains at a concentration of 1×10^6 cells per milliliter and incubated at 30 °C for 6 h (shaking at 220 rpm for 3 h and standing for 3 h). Protein extraction was performed using 250 μL of lysis buffer as described by Pandey et al. (58), without the addition of phosphatase inhibitors. Immunoprecipitation from supernatants was performed using Protein G Dynabeads (Life Technologies) according to the manufacturer's instructions. Dimethylpimelimidate was used to covalently bind mouse anti-GFP antibody (Life Technologies) or rabbit anti-mCherry antibody (BioVision) to the beads.

Bulked Segregant Analyses and Genome Resequencing. Bulked segregant analysis was performed as described by Heller et al. (17), with minor modifications. Genomic DNA was isolated from 50 progeny that underwent viable fusions with FGSC 2489, but not with segregant 2, and from 50 progeny that underwent viable fusions with segregant 2 but not with FGSC 2489. Equal amounts of DNA from 50 segregants (60 ng per segregant) were combined and used for library preparations. All paired-end libraries were sequenced on a HiSeq2000 sequencing platform using standard Illumina operating procedures (Vincent J. Coates Genomics Sequencing Laboratory, University of California, Berkeley). The mapped reads for each group of 50 pooled segregants are available at the Sequence Read Archive (SRP121656; https://www.ncbi.nlm.nih.gov/sra).

Sequence Analysis. The *sec-9*, *plp-1*, and *plp-2* sequences of *N. crassa* and *N. discreta* wild isolates were obtained by a BLAST search (59) using NCU09243, NCU09244, and NCU09245 from FGSC 2489 as a query against de novo sequence assemblies from 26 wild isolates (18, 25). Introns in sequences that had no ortholog in the reference genome (i.e., *plp-1.1*, *plp-1.2*) were identified independently for each GRDH using AUGUSTUS (60). For phylogenetic analyses, codon alignments were carried out using MACSE (61) and visualized and processed using Jalview (www.jalview.org/). Modified multiple alignments were trimmed using trimAl (62). Phylogenetic trees were inferred from trimmed alignments using the default pipeline from Phylogeny.fr [MUSCLE, Gblocks, phyML (100 bootstraps)] (63) and visualized using FigTree v1.4 (tree.bio.ed.ac.uk/software/figtree/). For population genetics analyses, sequences were manually assembled and aligned independently for each locus and each GRDH in Codoncode Aligner version 5.1.4 (www.codoncode.com/aboutus.htm). Sequences were then combined by pairs of haplogroups, by pairs of paralogs, or for each locus, and realigned using MAFFT with the E-INS-I option recommended for sequences with multiple conserved domains and long gaps (64). Summary statistics of polymorphism and divergence were computed using EggLib v3 (65).

ACKNOWLEDGMENTS. We thank the Berkeley Flow Cytometry Facility at the Cancer Research Laboratory, the Robert D. Ogg Electron Microscope Laboratory, and the Biological Imaging Facility [University of California (UC), Berkeley] for their technical support. We acknowledge the use of deletion strains generated by Grant P01 GM068087 "Functional Analysis of a Model Filamentous Fungus," which are publicly available at the FGSC. We also thank Dr. Trevor Starr for providing the plasmid pTSL88F. This work was funded by National Institute of General Medical Sciences Grant R01 GM060468 and by the Laboratory Directed Research and Development Program of Lawrence Berkeley National Laboratory under US Department of Energy Contract DE-AC02-05CH11231 (to N.L.G.). J.H. was supported by a research fellowship from the Deutsche Forschungsgemeinschaft (HE 7254/1-1). This work used the Vincent J. Coates Genomics Sequencing Laboratory (UC, Berkeley), supported by NIH S10 Instrumentation Grants S10RR029668 and S10RR027303.

1. Mekhedov SL, Makarova KS, Koonin EV (2017) The complex domain architecture of SAMD9 family proteins, predicted STAND-like NTPases, suggests new links to inflammation and apoptosis. *Biol Direct* 12:13.
2. Duxbury Z, et al. (2016) Pathogen perception by NLRs in plants and animals: Parallel worlds. *BioEssays* 38:769–781.
3. Jones JD, Vance RE, Dangl JL (2016) Intracellular innate immune surveillance devices in plants and animals. *Science* 354:aaf6395.
4. LaRock CN, Cookson BT (2013) Burning down the house: Cellular actions during pyroptosis. *PLoS Pathog* 9:e1003793.
5. da Silva Correia J, Miranda Y, Leonard N, Hsu J, Ulevitch RJ (2007) Regulation of Nod1-mediated signaling pathways. *Cell Death Differ* 14:830–839.
6. Urbach JM, Ausubel FM (2017) The NBS-LRR architectures of plant R-proteins and metazoan NLRs evolved in independent events. *Proc Natl Acad Sci USA* 114:1063–1068.

7. Daskalov A, Heller J, Herzog S, Fleißner A, Glass NL (2017) Molecular mechanisms regulating cell fusion and heterokaryon formation in filamentous fungi. *Microbiol Spectr* 5, 10.1128/microbiolspec.FUNK-0015-2016.
8. Saupe SJ (2000) Molecular genetics of heterokaryon incompatibility in filamentous ascomycetes. *Microbiol Mol Biol Rev* 64:489–502.
9. Biella S, Smith ML, Aist JR, Cortesi P, Milgroom MG (2002) Programmed cell death correlates with virus transmission in a filamentous fungus. *Proc Biol Sci* 269: 2269–2276.
10. Dyrka W, et al. (2014) Diversity and variability of NOD-like receptors in fungi. *Genome Biol Evol* 6:3137–3158.
11. Paoletti M, Saupe SJ (2009) Fungal incompatibility: Evolutionary origin in pathogen defense? *BioEssays* 31:1201–1210.
12. Jones JDG, Dangl JL (2006) The plant immune system. *Nature* 444:323–329.
13. Chae E, et al. (2014) Species-wide genetic incompatibility analysis identifies immune genes as hot spots of deleterious epistasis. *Cell* 159:1341–1351.
14. Danot O, Marquenet E, Vidal-Ingigliardi D, Richet E (2009) Wheel of life, wheel of death: A mechanistic insight into signaling by STAND proteins. *Structure* 17:172–182.
15. Saleh A, Srinivasula SM, Acharya S, Fishel R, Alnemri ES (1999) Cytochrome c and dATP-mediated oligomerization of Apaf-1 is a prerequisite for procaspase-9 activation. *J Biol Chem* 274:17941–17945.
16. DeYoung BJ, Innes RW (2006) Plant NBS-LRR proteins in pathogen sensing and host defense. *Nat Immunol* 7:1243–1249.
17. Heller J, et al. (2016) Characterization of greenbeard genes involved in long-distance kind discrimination in a microbial eukaryote. *PLoS Biol* 14:e1002431.
18. Zhao J, et al. (2015) Identification of allorecognition loci in *Neurospora crassa* by genomics and evolutionary approaches. *Mol Biol Evol* 32:2417–2432.
19. Galagan JE, et al. (2003) The genome sequence of the filamentous fungus *Neurospora crassa*. *Nature* 422:859–868.
20. Williams DC, Novick PJ (2009) Analysis of SEC9 suppression reveals a relationship of SNARE function to cell physiology. *PLoS One* 4:e5449.
21. Choi GH, et al. (2012) Molecular characterization of vegetative incompatibility genes that restrict hypovirus transmission in the chestnut blight fungus *Cryphonectria parasitica*. *Genetics* 190:113–127.
22. Arbogast BS, Edwards SV, Wakeley J, Beerli P, Slowinski JB (2002) Estimating divergence times from molecular data on phylogenetic and population genetic timescales. *Annu Rev Ecol Syst* 33:707–740.
23. Corcoran P, et al. (2014) A global multilocus analysis of the model fungus *Neurospora* reveals a single recent origin of a novel genetic system. *Mol Phylogenet Evol* 78: 136–147.
24. Ellison CE, et al. (2011) Population genomics and local adaptation in wild isolates of a model microbial eukaryote. *Proc Natl Acad Sci USA* 108:2831–2836.
25. Gladieux P, et al. (2015) Genomic sequencing reveals historical, demographic and selective factors associated with the diversification of the fire-associated fungus *Neurospora discreta*. *Mol Ecol* 24:5657–5675.
26. Hall C, Welch J, Kowbel DJ, Glass NL (2010) Evolution and diversity of a fungal self/nonself recognition locus. *PLoS One* 5:e14055.
27. Brennwald P, et al. (1994) Sec9 is a SNAP-25-like component of a yeast SNARE complex that may be the effector of Sec4 function in exocytosis. *Cell* 79:245–258.
28. Katz L, Hanson PI, Heuser JE, Brennwald P (1998) Genetic and morphological analyses reveal a critical interaction between the C-termini of two SNARE proteins and a parallel four helical arrangement for the exocytic SNARE complex. *EMBO J* 17: 6200–6209.
29. Rydel TJ, et al. (2003) The crystal structure, mutagenesis, and activity studies reveal that patatin is a lipid acyl hydrolase with a Ser-Asp catalytic dyad. *Biochemistry* 42: 6696–6708.
30. Martinon F, Tschopp J (2005) NLRs join TLRs as innate sensors of pathogens. *Trends Immunol* 26:447–454.
31. Aanen DK, Debets AJ, de Visser JA, Hoekstra RF (2008) The social evolution of somatic fusion. *BioEssays* 30:1193–1203.
32. Rinkevich B (2004) Primitive immune systems: Are your ways my ways? *Immunol Rev* 198:25–35.
33. Sijacic P, et al. (2004) Identification of the pollen determinant of S-RNase-mediated self-incompatibility. *Nature* 429:302–305.
34. Chantha SC, Herman AC, Platts AE, Vekemans X, Schoen DJ (2013) Secondary evolution of a self-incompatibility locus in the Brassicaceae genus Leavenworthia. *PLoS Biol* 11:e1001560.
35. McKitrick TR, De Tomaso AW (2010) Molecular mechanisms of allorecognition in a basal chordate. *Semin Immunol* 22:34–38.
36. Bentham A, Burdett H, Anderson PA, Williams SJ, Kobe B (2017) Animal NLRs provide structural insights into plant NLR function. *Ann Bot* 119:827–702.
37. Kim DS, Jeun Y, Hwang BK (2014) The pepper patatin-like phospholipase CaPLP1 functions in plant cell death and defense signaling. *Plant Mol Biol* 84:329–344.
38. La Camera S, et al. (2009) The *Arabidopsis* patatin-like protein 2 (PLP2) plays an essential role in cell death execution and differentially affects biosynthesis of oxylipins and resistance to pathogens. *Mol Plant Microbe Interact* 22:469–481.
39. El Kasmi F, et al. (2017) Signaling from the plasma-membrane localized plant immune receptor RPM1 requires self-association of the full-length protein. *Proc Natl Acad Sci USA* 114:E7385–E7394.
40. Nair U, et al. (2011) SNARE proteins are required for macroautophagy. *Cell* 146: 290–302.
41. Wesolowski J, Paumet F (2010) SNARE motif: A common motif used by pathogens to manipulate membrane fusion. *Virulence* 1:319–324.
42. Shi X, Halder P, Yavuz H, Jahn R, Shuman HA (2016) Direct targeting of membrane fusion by SNARE mimicry: Convergent evolution of *Legionella* effectors. *Proc Natl Acad Sci USA* 113:8807–8812.
43. Delevoye C, et al. (2008) SNARE protein mimicry by an intracellular bacterium. *PLoS Pathog* 4:e1000022.
44. Arasaki K, et al. (2017) *Legionella* effector Lpg1137 shuts down ER-mitochondria communication through cleavage of syntaxin 17. *Nat Commun* 8:15406.
45. Du Y, Mpina MH, Birch PR, Bouwmeester K, Govers F (2015) *Phytophthora infestans* RXLR effector AVR1 interacts with exocyst component Sec5 to manipulate plant immunity. *Plant Physiol* 169:1975–1990.
46. Yun HS, Kang BG, Kwon C (2016) *Arabidopsis* immune secretory pathways to powdery mildew fungi. *Plant Signal Behav* 11:e1226456.
47. Fujisaki K, et al. (2015) Rice Exo70 interacts with a fungal effector, AVR-Pii, and is required for AVR-Pii-triggered immunity. *Plant J* 83:875–887.
48. Vogel HJ (1956) A convenient growth medium for *Neurospora*. *Microb Genet Bull* 13: 42–46.
49. Westergaard M, Mitchell HK (1947) *Neurospora* V. A synthetic medium favoring sexual reproduction. *Am J Bot* 34:573–577.
50. Colot HV, et al. (2006) A high-throughput gene knockout procedure for *Neurospora* reveals functions for multiple transcription factors. *Proc Natl Acad Sci USA* 103: 10352–10357.
51. Dunlap JC, et al. (2007) Enabling a community to dissect an organism: Overview of the *Neurospora* functional genomics project. *Adv Genet* 57:49–96.
52. Szewczyk E, et al. (2006) Fusion PCR and gene targeting in *Aspergillus nidulans*. *Nat Protoc* 1:3111–3120, and erratum (2006) 1:following 31120.
53. Freitag M, Hickey PC, Raju NB, Selker EU, Read ND (2004) GFP as a tool to analyze the organization, dynamics and function of nuclei and microtubules in *Neurospora crassa*. *Fungal Genet Biol* 41:897–910.
54. Jonkers W, et al. (2014) HAM-5 functions as a MAP kinase scaffold during cell fusion in *Neurospora crassa*. *PLoS Genet* 10:e1004783.
55. Bardiya N, Shiu PK (2007) Cyclosporin A-resistance based gene placement system for *Neurospora crassa*. *Fungal Genet Biol* 44:307–314.
56. El-Khoury R, et al. (2008) Gene deletion and allelic replacement in the filamentous fungus *Podospora anserina*. *Curr Genet* 53:249–258.
57. Fleissner A, Diamond S, Glass NL (2009) The *Saccharomyces cerevisiae* PRM1 homolog in *Neurospora crassa* is involved in vegetative and sexual cell fusion events but also has postfertilization functions. *Genetics* 181:497–510.
58. Pandey A, Roca MG, Read ND, Glass NL (2004) Role of a mitogen-activated protein kinase pathway during conidial germination and hyphal fusion in *Neurospora crassa*. *Eukaryot Cell* 3:348–358.
59. Altschul SF, Gish W, Miller W, Myers EW, Lipman DJ (1990) Basic local alignment search tool. *J Mol Biol* 215:403–410.
60. Stanke M, Morgenstern B (2005) AUGUSTUS: A web server for gene prediction in eukaryotes that allows user-defined constraints. *Nucleic Acids Res* 33:W465–W467.
61. Ranwez V, Harispe S, Delsuc F, Douzery EJ (2011) MACSE: Multiple Alignment of Coding SEquences accounting for frameshifts and stop codons. *PLoS One* 6:e22594.
62. Capella-Gutiérrez S, Silla-Martínez JM, Gabaldón T (2009) trimAl: A tool for automated alignment trimming in large-scale phylogenetic analyses. *Bioinformatics* 25: 1972–1973.
63. Dereeper A, et al. (2008) Phylogeny.fr: Robust phylogenetic analysis for the non-specialist. *Nucleic Acids Res* 36:W465–W469.
64. Katoh K, Standley DM (2013) MAFFT multiple sequence alignment software version 7: Improvements in performance and usability. *Mol Biol Evol* 30:772–780.
65. De Mita S, Siol M (2012) EggLib: Processing, analysis and simulation tools for population genetics and genomics. *BMC Genet* 13:27.